Magnetic-proximity-induced magnetoresistance on topological insulators

Chiba, Takahiro; Takahashi, Saburo; Bauer, Gerrit E.W.

DOI
10.1103/PhysRevB.95.094428

Publication date
2017

Document Version
Final published version

Published in
Physical Review B (Condensed Matter and Materials Physics)

Magnetic-proximity-induced magnetoresistance on topological insulators

Takahiro Chiba,[1,*] Saburo Takahashi,[1] and Gerrit E. W. Bauer[1,2,3]
[1]*Institute for Materials Research, Tohoku University, Sendai 980-8577, Japan*
[2]*WPI-AIMR, Tohoku University, Sendai 980-8577, Japan*
[3]*Kavli Institute of NanoScience, Delft University of Technology, Lorentzweg 1, 2628 CJ Delft, The Netherlands*
(Received 13 December 2016; published 28 March 2017)

We theoretically study the magnetoresistance (MR) of two-dimensional massless Dirac electrons as found on the surface of three-dimensional topological insulators (TIs) that are capped by a ferromagnetic insulator (FI). We calculate charge and spin transport by Kubo and Boltzmann theories, taking into account the ladder-vertex correction and the in-scattering due to normal and magnetic disorder. The induced exchange splitting is found to generate an electric conductivity that depends on the magnetization orientation, but its form is very different from both the anisotropic and the spin Hall MR. The in-plane MR vanishes identically for nonmagnetic disorder, while out-of-plane magnetizations cause a large MR ratio. On the other hand, we do find an in-plane MR and planar Hall effect in the presence of magnetic disorder aligned with the FI magnetization. Our results may help us understand recent transport measurements on TI|FI systems.

DOI: 10.1103/PhysRevB.95.094428

I. INTRODUCTION

The control of electric transport by utilizing the spin angular momentum has been a central theme in spintronics after the discovery of the giant and tunnel magnetoresistances, leading to new functionalities for sensing, logic, and data storage applications [1]. On the other hand, the anisotropic magnetoresistance (AMR) in ferromagnets, i.e., the dependence of electric transport on the relative angle between the current and magnetization directions, has already been discovered in 1857 by Lord Kelvin [2]. Just like the anomalous Hall effect (AHE), it is rooted in the spin-orbit coupling (SOC). In the absence of a general theory, several studies addressed the AMR in a simple model system, viz., the two-dimensional (2D) electron gas with Rashba and Dresselhaus SOCs. The applied methods were the Boltzmann equation [3,4] and the linear-response Kubo formalism [5,6].

Recently, a so-called spin Hall magnetoresistance (SMR) has been discovered in bilayers made from heavy normal metals such as platinum and ferromagnetic insulators (FIs) such as $Y_3Fe_5O_{12}$ (YIG) [7,8]. The SMR can be explained by the simultaneous action of the spin Hall effect (SHE) [9] and its inverse that is modulated by the spin transfer torque or the relative angle of the current-induced spin polarization in the metal and the magnetization direction of the ferromagnet. Hence, the SMR is a nonlocal and nonequilibrium magnetic proximity effect (MPE). Alternative mechanisms for the SMR have been proposed, i.e., the magnetized normal metal, typically Pt, by the ferromagnet contact [10] or the Rashba SOC at the interface [11,12], but theoretical and experimental support of those models is still scarce. SMR-like phenomena have been observed for all metallic bilayers as well [13,14], but the interpretation of the results is easier when the magnet is an electric insulator since parallel current paths through the magnet can be excluded. The reported SMR ratios are quite small (of the order of 10^{-4}), being proportional to the squared spin Hall angle which is typically less than 10% [9].

Three-dimensional topological insulators (3D TIs) are ideally insulating in the bulk while supporting topologically protected metallic surface states as a consequence of time-reversal symmetry and band inversion induced by a strong SOC [15–17]. In the surface of TIs as well as the Rashba-splitting 2D electron gas (2DEG), the helical band structure is realized, in which the spin and momentum are locked and hence the surface currents are spin polarized [18–20]. The interface between a TI (or a Rashba 2DEG [21]) and a ferromagnet can be a spin source in which the SOC enhances the magnitude of both charge and spin currents [22–25]. Electric transport properties of bilayers of 3D TIs with (metallic) ferromagnets have indeed been interpreted in terms of much larger spin Hall angles [26,27]. Recently, there have been some experiments with YIG for the spin-charge conversion [28,29]. TIs are therefore a promising platform to enhance the SMR.

The SMR interpretation in terms of SHE and inverse SHE is based on a semiclassical spin diffusion model and does not hold for 2D materials. Since the transport is confined now to an atomic monolayer, a MR generated by an induced proximity exchange potential (or equilibrium MPE) appears plausible [30–33]. In 3D systems this effective interface magnetic field is proportional to the imaginary part of the mixing conductance [34] that for an interface between a FI and a nonmagnetic metal is relatively small and is usually disregarded [35]. For graphene on YIG, a proximity potential of 20 μeV (0.2 T) has been reported [32], which is smaller than predicted [36]. A much larger proximity potential of 14 meV (14 T) has been reported for graphene on EuS [33].

Despite the progress in understanding the magnetoresistance (MR) of a magnetized 2DEG with Rashba SOC and the large attention for the AHE in Zeeman-split TI surface states, a thorough discussion of the AMR/SMR of the latter appears to be lacking. We therefore report here a theory of the MR of a TI|FI bilayer, modeled as a 2D Dirac system with finite exchange splitting, where the latter is a vector parallel to the FI magnetization that can be controlled by applied magnetic fields [31,33]. We calculate the electric dc conductivity in a magnetized 2D Dirac electron system by the Kubo formalism

*t.chiba@imr.tohoku.ac.jp

and the linearized Boltzmann equation with random potential disorder. The equilibrium magnetic proximity effect, i.e., the exchange interaction in the surface state induced by an attached magnet, is found to generate a MR that depends on the magnetization orientation. However, its form differs from both AMR and SMR. For in-plane magnetizations the MR vanishes identically in the TI|FI bilayer, while an out-of-plane magnetization causes a large MR ratio. Moreover, we do find an in-plane MR and a planar Hall effect in the presence of magnetic disorder when aligned with the FI magnetization. Our calculated results agree well with the MR observations. We also discuss the current-induced spin polarization and the role of magnetic impurities.

In Sec. II, we present a model for the surface of TIs with a finite exchange potential controlled by an FI contact. In Sec. III, we calculate the electric dc conductivity in magnetized 2D Dirac electrons with randomly distributed nonmagnetic disorder by the Kubo formalism. In Sec. IV, we address the same problem by the linearized Boltzmann equation and get identical results. We also discuss the current-induced spin polarization. In Sec. V, we address the effect of magnetic impurities on electric transport and briefly discuss the related MR experiments on TI. We summarize the results and conclusions in Sec. VI.

II. TWO-DIMENSIONAL MASSLESS DIRAC MODEL

We consider 2D massless Dirac electrons on the surface of the TI, exchange-coupled to a homogeneous magnetization of an attached FI, as shown in Fig. 1. A simple model for the electronic structure of a TI surface state is the massless Dirac Hamiltonian [15]. When the TI electrons are in contact with an FI [30], they experience an exchange interaction that can be modeled by a constant spin splitting Δ along the magnetization direction with unit vector $\mathbf{M}$ [37]. Our model Hamiltonian is hence

$$\hat{H} = -i\hbar v_F \hat{\boldsymbol{\sigma}} \cdot (\nabla \times \hat{\mathbf{z}}) + \Delta \hat{\boldsymbol{\sigma}} \cdot \mathbf{M}, \tag{1}$$

where v_F is the Fermi velocity of the Dirac fermions propagating with momentum $\hbar\mathbf{k}$ measured relative to the Γ point of the surface Brillouin zone. For Bi_2Te_3 the Fermi velocity is $v_F = 4.3 \times 10^5$ m/s [16]. Here, $\hat{\boldsymbol{\sigma}}$ is the Pauli matrix operator and Δ the proximity-induced exchange energy. Equation (1) leads to the energy dispersion

$$E_{ks} = s\sqrt{(\hbar v_F k_x + \Delta M_y)^2 + (\hbar v_F k_y - \Delta M_x)^2 + (\Delta M_z)^2}, \tag{2}$$

where $s = \pm$ corresponds to the upper and lower bands. For an in-plane exchange field we can rewrite Eq. (1) as $\hat{H} = v_F(-i\hbar\nabla - e\mathbf{A}) \cdot (\hat{\mathbf{z}} \times \hat{\boldsymbol{\sigma}}) + \Delta M_z \hat{\sigma}_z$. The vector potential $\mathbf{A} = -\Delta/(ev_F)\mathbf{M} \times \hat{\mathbf{z}}$ shifts the position of the Dirac point in the (k_x,k_y) plane and the electron charge is $-e$. A uniform and static $\mathbf{A}$ can be removed by the gauge transformation $(k_x,k_y) \to (q_x + eA_x/\hbar, q_y + eA_y/\hbar)$ and hence does not affect the physical observables. The energy dispersion is then $E_{qs} = s\sqrt{(\hbar v_F)^2(q_x^2 + q_y^2) + (\Delta M_z)^2}$ and eigenfunctions can

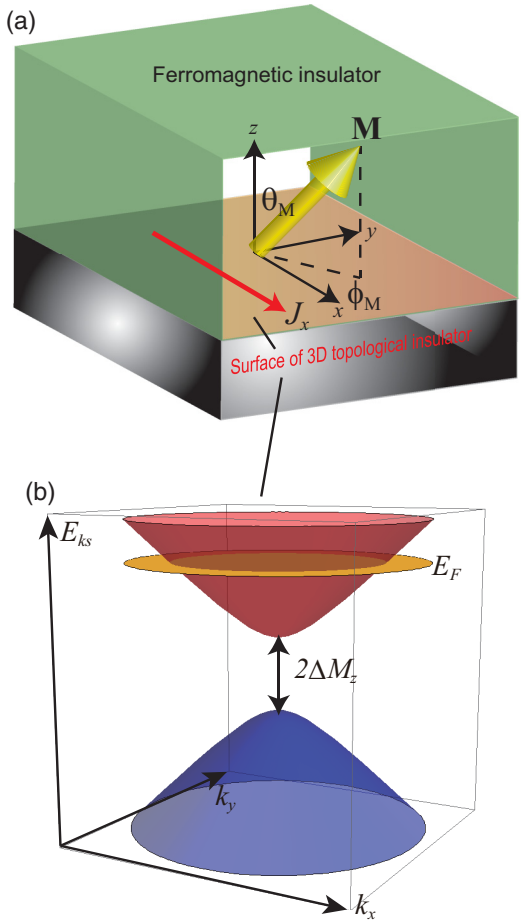

FIG. 1. (a) Bilayer of a three-dimensional topological insulator and a ferromagnetic insulator. Electric currents flow on the surface of the TI in proximity to the magnet (shown as the red area). (b) Schematic energy dispersion of the gapped 2D Dirac Hamiltonian. The Fermi level is taken to be above the gap.

be written as $\psi_{qs} = e^{i\mathbf{q}\cdot\mathbf{r}}|u_{qs}\rangle$, with

$$|u_{q+}\rangle = \begin{pmatrix} \cos(\theta/2) \\ -ie^{i\phi}\sin(\theta/2) \end{pmatrix}, \quad |u_{q-}\rangle = \begin{pmatrix} \sin(\theta/2) \\ ie^{i\phi}\cos(\theta/2) \end{pmatrix}, \tag{3}$$

where $\cos\theta = \Delta M_z/|E_{qs}|$ and $\tan\phi = q_y/q_x$ determine the polar angle and the azimuth of the spinors on the Bloch sphere.

The electron density of massless Dirac electrons relative to the neutrality point reads

$$n_e = \int_0^{E_F^{(0)}} dE\, D_0(E) = \frac{\left(E_F^{(0)}\right)^2}{4\pi(\hbar v_F)^2}, \tag{4}$$

where $D_0(E) = \sum_{qs}\delta(E_{qs} - E) = E/[2\pi(\hbar v_F)^2]$ is the density of states per unit area. $E_F^{(0)} = \hbar v_F\sqrt{4\pi n_e}$ is the Fermi energy for the gapless dispersion or in-plane magnetization. When the electron density n_e is kept constant under a rotating magnetization, the Fermi energy of the gapped state reads $E_F(M_z) = E_F^{(0)}\sqrt{1 + \zeta^2 M_z^2}$, with $\zeta = \Delta/E_F^{(0)}$.

III. THE KUBO FORMULA

The MR is accessed in linear current response to an applied voltage (Ohm's law). Here we calculate electric dc conductivity in a magnetized 2D Dirac electron system with nonmagnetic disorder by the Kubo formalism. We assume that transport is limited by a randomly distributed disorder potential,

$$\hat{V}(\mathbf{r}) = V_0 \sum_{i=1}^{N} \delta(\mathbf{r} - \mathbf{R}_i), \tag{5}$$

that is weak, and short-range Gaussian correlated $\langle \hat{V}(\mathbf{r}_1)\hat{V}(\mathbf{r}_2)\rangle_{\rm imp} = nV_0^2\delta(\mathbf{r}_1 - \mathbf{r}_2)$, with impurity concentration n and (normal) scattering potential V_0. In writing the impurity potentials as 2D δ functions, we implicitly integrated over the envelope function of the TI surface state thereby including bulk impurities close to the interface. We focus on the dc conductivity of Zeeman-split 2D Dirac electrons at zero temperature expressed in terms of the retarded and advanced Green functions. This approach has previously been applied to, e.g., the AHE [38–40] and the AMR [5] for spin-polarized 2D electrons with Rashba SOC. In the diffusive transport regime, the Kubo formula for the dc conductivity can be written as

$$\sigma_{xv} = \frac{\hbar}{2\pi L^2} \mathrm{Tr}\langle \hat{j}_x \hat{G}^R \hat{j}_v \hat{G}^A\rangle_{\rm imp}, \tag{6}$$

where L^2 is the system area and $\hat{G}^{R(A)}(\epsilon) = (\epsilon \pm i0 - \hat{H} - \hat{V})^{-1}$ is the retarded (advanced) Green function in the Pauli spin space. The current operator reads $\hat{\mathbf{j}} = -e(-i/\hbar)[\hat{\mathbf{r}}, \hat{H}] = -ev_F\hat{\mathbf{z}}\times\hat{\boldsymbol{\sigma}}$. Here $\langle\cdots\rangle_{\rm imp}$ indicates an ensemble average over random realizations of the impurity potential that we treat in the Born approximation for the self-energy and the ladder approximation for the current vertex [5]. The conductivity then reads

$$\begin{aligned}\sigma_{xv} &\approx \frac{\hbar}{2\pi L^2} \mathrm{Tr}[\hat{j}_x\langle\hat{G}^R\rangle\hat{j}_v\langle\hat{G}^A\rangle] + \text{Vertex correction} \\ &\equiv \frac{\hbar}{2\pi L^2} \mathrm{Tr}[\hat{j}_x\langle\hat{G}^R\rangle\hat{J}_v\langle\hat{G}^A\rangle],\end{aligned} \tag{7}$$

where $\langle\hat{G}^{R(A)}\rangle$ is the averaged Green function and $\hat{J}_v$ the corrected current vertex that includes the diffuse scattering from impurities. The latter vanishes for short-range impurity scattering in simple electron gases, but can be important in the presence of impurity scattering, leading for instance to the dephasing of the intrinsic spin Hall effect in the Rashba 2DEG [41]

A. Self-energy

Here we calculate the averaged Green function by solving the Dyson equation in the Born approximation as shown in Fig. 2. Hence, the averaged Green function can be written as

$$\begin{aligned}\langle\hat{G}^{R(A)}\rangle &= \langle(z - \hat{H} - \hat{V})^{-1}\rangle_{\rm imp} \\ &= \hat{G}_0^{R(A)} + \hat{G}_0^{R(A)}\hat{\Sigma}^{R(A)}\langle\hat{G}^{R(A)}\rangle,\end{aligned} \tag{8}$$

with $z = \epsilon \pm i0$. The solution to this equation is

$$\langle\hat{G}^{R(A)}\rangle = \left(\left(\hat{G}_0^{R(A)}\right)^{-1} - \hat{\Sigma}^{R(A)}\right)^{-1}, \tag{9}$$

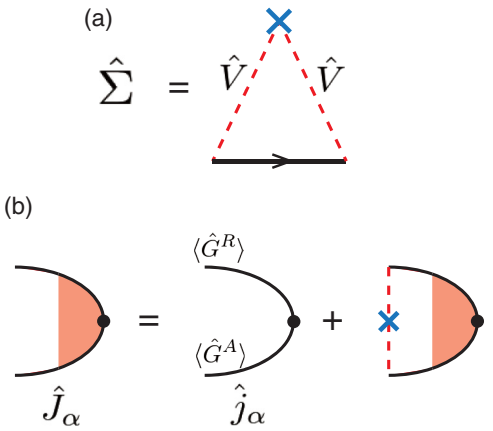

FIG. 2. (a) Self-energy diagram in the Born approximation. (b) The current vertex correction is the geometric sum of ladder diagrams.

with the self-energy being

$$\hat{\Sigma}^{R(A)} = \langle\hat{V}\rangle_{\rm imp} + \left\langle\hat{V}\hat{G}_0^{R(A)}\hat{V}\right\rangle_{\rm imp}, \tag{10}$$

and the constant average $\langle\hat{V}\rangle_{\rm imp}$ is absorbed in the Fermi energy E_F in the following. In terms of the unperturbed Green function,

$$\hat{G}_0^{R(A)} = \sum_{qs}(\epsilon - E_{qs} \pm i0)^{-1}|u_{qs}\rangle\langle u_{qs}|, \tag{11}$$

$$\left\langle\hat{V}\hat{G}_0^{R(A)}\hat{V}\right\rangle_{\rm imp} = nV_0^2\int\frac{d^2\mathbf{q}}{(2\pi)^2}\hat{G}_0^{R(A)} = \mp i\frac{\hbar}{4\tau_{\rm e}}(1 + \xi M_z\hat{\sigma}_z), \tag{12}$$

where $1/\tau_{\rm e} = nV_0^2\int_0^\infty qdq\delta(E_F - E_{q+})/\hbar = 2\pi nV_0^2D(E_F)/\hbar = 2\pi nV_0^2E_F/[h(\hbar v_F)^2]$ denotes the elastic scattering rate and $\xi = \Delta/E_F = \zeta/\sqrt{1 + \zeta^2M_z^2}$. Equation (12) shows how the self energy is modulated by the magnetization direction. Hence, the averaged Green function is

$$\langle\hat{G}^{R(A)}\rangle = \frac{\varepsilon \pm i\Gamma_0 + \hbar v_F\mathbf{q}\cdot(\hat{z}\times\hat{\boldsymbol{\sigma}}) + (\Delta M_z \mp i\Gamma_1)\hat{\sigma}_z}{(\varepsilon - E_{\mathbf{q}}^+ \pm i\gamma^+)(\varepsilon - E_{\mathbf{q}}^- \pm i\gamma^-)}, \tag{13}$$

where $\Gamma_0 = 1/(4\tau_{\rm e})$, $\Gamma_1 = \Gamma_0\cos\theta$, and $\gamma^\pm = \Gamma_0(1 \pm \cos^2\theta)$.

B. Current vertex correction

The vertex function in the Born approximation is represented by the sum of all ladder diagrams in Fig. 2. The self-consistent Born approximation of the self-energy is consistent with the ladder approximation to the vertex correction, while the first-order Born approximation holds in the limit of weak disorder. This correspondence has been confirmed for the AHE [42,43]. Hence, we treat the AMR within the ladder approximation and the first-order Born approximation, which leads to an analytical formula for the conductivity that agrees with the solution of the Boltzmann equation (see below).

The ladder-type vertex-corrected current operator $\hat{J}_v$ in Fig. 2 obeys the integral (Bethe-Salpeter) equation [42–45]

$$\hat{J}_v = \hat{j}_v + nV_0^2\int\frac{d^2\mathbf{q}}{(2\pi)^2}\langle\hat{G}^R\rangle\hat{J}_v\langle\hat{G}^A\rangle. \tag{14}$$

By iteration and Eq. (13), the first-order single-impurity vertex correction reads

$$\hat{J}_\nu^{(1)} = nV_0^2 \int \frac{d^2\mathbf{q}}{(2\pi)^2} \langle \hat{G}^R \rangle \hat{j}_\nu \langle \hat{G}^A \rangle = -ev(\mp A\hat{\sigma}_\nu + B\hat{\sigma}_{\bar{\nu}}) \tag{15}$$

($-$ for $\nu = x, \bar{\nu} = y$ and $+$ for $\nu = y, \bar{\nu} = x$), with

$$A = \frac{1-\xi^2 M_z^2}{2\left(1+\xi^2 M_z^2\right)},\ B = \frac{\hbar}{E_F\tau_e}\frac{\xi M_z}{2\left(1+\xi^2 M_z^2\right)}. \tag{16}$$

Expanding $\hat{J}_\nu = -ev_F \sum_i c_{\nu i}\hat{\sigma}_i$ in Eq. (14) as

$$\hat{J}_\nu = ev_F\left(\pm\hat{\sigma}_{\bar{\nu}} - nV_0^2 \sum_i \int \frac{d^2\mathbf{q}}{(2\pi)^2} \langle \hat{G}^R \rangle c_{\nu i}\hat{\sigma}_i \langle \hat{G}^A \rangle\right), \tag{17}$$

we find in the weak scattering limit

$$\begin{pmatrix} c_{\nu x} \\ c_{\nu y} \end{pmatrix} = \frac{1}{(1-A)^2}\begin{pmatrix} B & 1-A \\ -(1-A) & B \end{pmatrix}\begin{pmatrix} \delta_{x\nu} \\ \delta_{y\nu} \end{pmatrix} \tag{18}$$

and $c_{\nu 0} = c_{\nu z} = 0$, where $\delta_{x\nu}$ and $\delta_{y\nu}$ are the Kronecker δ. For the limit of $\hbar/(E_F\tau_e) \ll 1$, the renormalized current vertex reads

$$\begin{pmatrix} \hat{J}_x \\ \hat{J}_y \end{pmatrix} = -ev_F\begin{pmatrix} -a & b \\ b & a \end{pmatrix}\begin{pmatrix} \hat{\sigma}_y \\ \hat{\sigma}_x \end{pmatrix}, \tag{19}$$

with

$$a = c_{yx} = -c_{xy} = 2\frac{1+\xi^2 M_z^2}{1+3\xi^2 M_z^2},$$
$$b = c_{xx} = c_{yy} = 2\frac{\hbar}{E_F\tau_e}\frac{\xi M_z\left(1+\xi^2 M_z^2\right)}{\left(1+3\xi^2 M_z^2\right)^2}. \tag{20}$$

In the gapless limit of $\xi M_z \to 0$ this reduces to $a = 2$ and $b = 0$.

C. Longitudinal and transverse conductivities

Inserting Eqs. (13) and (19) into Eq. (7), we get

$$\sigma_{xx} = a\sigma_{xx}^{\rm nv} + b\sigma_{xy}^{\rm nv},\quad \sigma_{xy} = -b\sigma_{xx}^{\rm nv} + a\sigma_{xy}^{\rm nv}. \tag{21}$$

Here $\sigma_{x\nu}^{\rm nv} = \hbar\,{\rm Tr}\,[\hat{j}_x\langle\hat{G}^R\rangle\hat{j}_\nu\langle\hat{G}^A\rangle]/(2\pi L^2)$ are the longitudinal and transverse conductivities without vertex correction ("bare bubbles"):

$$\sigma_{xx}^{\rm nv} = \frac{e^2}{h}\frac{E_F\tau_e}{\hbar}\frac{1-\xi^2 M_z^2}{1+\xi^2 M_z^2},\quad \sigma_{xy}^{\rm nv} = -\frac{e^2}{2h}\frac{2\xi M_z}{1+\xi^2 M_z^2}. \tag{22}$$

When the gap vanishes with $\xi M_z \to 0$, the longitudinal and transverse conductivities reduce to

$$\sigma_{xx}^{\rm nv} = \frac{e^2}{h}\frac{E_F\tau_e}{\hbar} \tag{23}$$

and $\sigma_{xy}^{\rm nv} = 0$. Below we show that $\sigma_{xx}^{\rm nv}$ is half of the full (vertex-corrected) result [Eq. (26)]. This discrepancy reflects the inherent anisotropy of the scattering of Dirac fermions that affects the transport and relaxation times even for short-range correlated scattering. Substituting Eqs. (20) and (22) into Eq. (21), we get

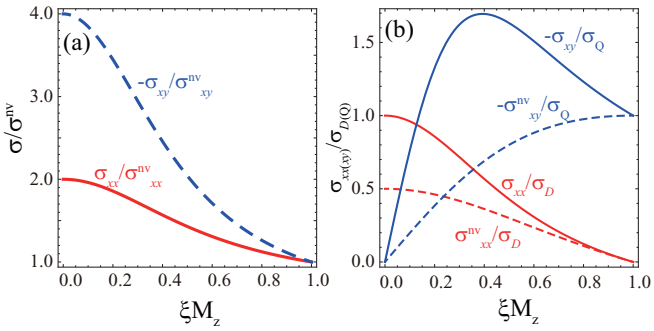

FIG. 3. (a) Ratio of the dc conductivities without ($\sigma_{x\alpha}^{\rm nv}$) and with vertex correction ($\sigma_{x\alpha}$) as a function of ξM_z. (b) The longitudinal and transverse conductivities without and with vertex correction as a function of ξM_z. $\sigma_D = (2e^2/h)(E_F\tau^e/\hbar)$ is the longitudinal conductivity of two-dimensional massless Dirac electrons without magnetic or exchange fields, while $\sigma_Q = e^2/(2h)$.

$$\sigma_{xx} = 2\frac{e^2}{h}\frac{E_F\tau_e}{\hbar}\frac{1-\xi^2 M_z^2}{1+3\xi^2 M_z^2}, \tag{24}$$

$$\sigma_{xy} = -\frac{e^2}{2h}\xi M_z\frac{8\left(1+\xi^2 M_z^2\right)}{\left(1+3\xi^2 M_z^2\right)^2}. \tag{25}$$

For $\xi M_z \to 0$,

$$\sigma_{xx} = 2\frac{e^2}{h}\frac{E_F\tau_e}{\hbar} \equiv \frac{e^2}{h}\frac{E_F\tau}{2\hbar} \tag{26}$$

and $\sigma_{xy} = 0$, where $\tau = 4\tau_e$ is the transport relaxation time of massless Dirac electrons. $\sigma_{xx}(\xi M_z = 0)$ is the longitudinal conductivity of nonmagnetic 2D massless Dirac electrons [46,47], which implies that the in-plane exchange potential has no effect on electron transport as expected from the gauge-field argument above. We here disregard the third-order "skew-scattering" term. Otherwise, our $\sigma_{xy}(M_z)$ agrees with previous results [42,44,48,49]. $\sigma_{xx}(M_z)$ has been derived in Ref. [49]. Figure 3(a) shows the ratio of the dc conductivities without and with the ladder-vertex correction as a function of ξM_z, while Fig. 3(b) is a plot of the ξM_z dependence of the conductivities $\sigma_{x\nu}$ and $\sigma_{x\nu}^{\rm nv}$. When the electron density [Eq. (4)] is kept constant for all $\mathbf{M}$, the longitudinal conductivity becomes

$$\sigma_{xx} = 2\frac{e^2}{h}\frac{E_F^{(0)}\tau_e^{(0)}}{\hbar}\frac{1}{1+4\zeta^2 M_z^2}, \tag{27}$$

where $1/(E_F^{(0)}\tau_e^{(0)}) = 2\pi n V_0^2/[h(\hbar v_F)^2] = 1/(E_F\tau_e)$. Hence, to leading order in $(\zeta M_z)^2$ the MRs for constant density or Fermi energy are the same.

D. Parameter dependence

Figures 4(a) and 4(b) show the longitudinal conductivity σ_{xx} as a function of angles α, β, and γ of the FI magnetization in the x-y, y-z, and x-z planes, respectively, while Fig. 4(c) shows the transverse conductivity σ_{xy} for different Fermi energies E_F. The calculated results for $\sigma_{xx} = \sigma_{xx}(M_z^2)$ are very similar to those computed for magnetically doped TIs [50]. The

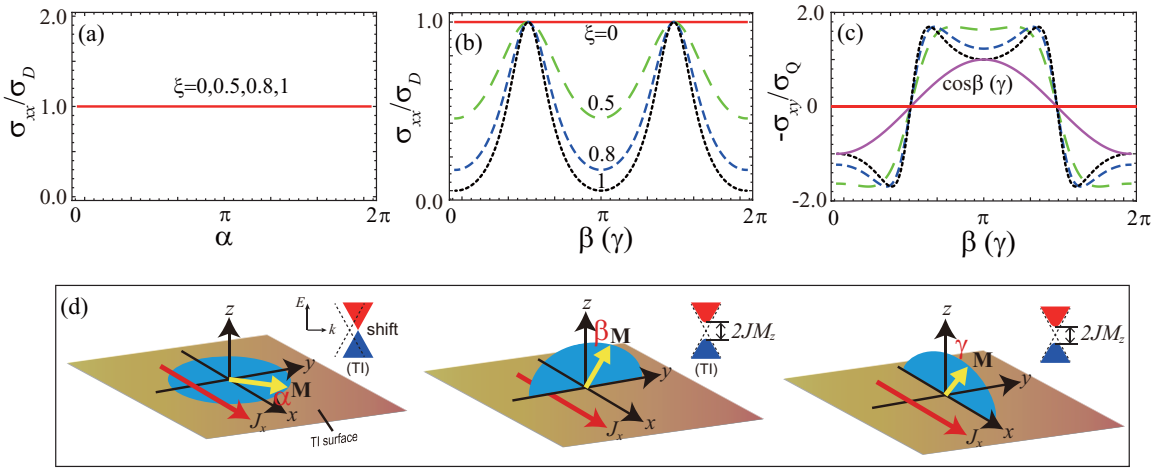

FIG. 4. Calculated conductivities in the TI|FI bilayer as a function of magnetization angles α, β, and γ [shown in panel (d)] and for different ratios $\xi = J/E_F$. Panels (a) and (b) show the longitudinal conductivity and panel (c) shows the transverse (Hall) conductivity. Each subplot in panel (d) shows a different configuration and associated band structure of the surface state. σ_D and σ_Q are defined in Fig. 3. The dependence on the angles β and γ is here the same. The $\cos\beta(\gamma)$ function is plotted in panel (c) for reference.

inset in each magnetization rotation in Fig. 4(d) illustrate the band structure: When the magnetization is in-plane, the bands are rigidly shifted in the k_x,k_y plane, which does not affect the MR. In contrast, an out-of-plane magnetization opens a gap that suppresses the longitudinal conductivity.

IV. BOLTZMANN TRANSPORT THEORY

A. Transport time

Here we employ the Boltzmann equation to calculate the electric dc conductivity of a magnetized 2D massless Dirac electron system with (initially) nonmagnetic disorder and arrive at results that are identical with those from the Kubo formalism in the previous section and Ref. [49]. We show that the in-scattering term of the collision integral in the Boltzmann theory is significant and equivalent with the current-vertex correction in the linear response theory (see Sec. III). Sufficiently far from the Dirac point the impurity scattering can be treated by the Born approximation [51]. The nonequilibrium distribution function $f(\mathbf{q})$ in the presence of a uniform external electric field $\mathbf{E}$ is governed by the linearized Boltzmann equation

$$-e\left(-\frac{\partial f^{(0)}}{\partial E_{qs}}\right)\mathbf{v}_{qs}\cdot\mathbf{E} = \left(\frac{\partial f}{\partial t}\right)_{\rm scat}, \tag{28}$$

where $\mathbf{v}_{qs} = \nabla_{\mathbf{q}}E_{qs}/\hbar$ is the group velocity and $f^{(0)}(\mathbf{q})$ the equilibrium Fermi-Dirac distribution function. The collision term on the right-hand side is affected by in- and out-scattering of the state with wave vector $\mathbf{q}$:

$$\left(\frac{\partial f}{\partial t}\right)_{\rm scat} = \frac{1}{L^2}\sum_{\mathbf{q}'} W_{\mathbf{q},\mathbf{q}'}[f(\mathbf{q}') - f(\mathbf{q})], \tag{29}$$

where $W_{\mathbf{q},\mathbf{q}'}$ is the transition probability between $\mathbf{q}$ and $\mathbf{q}'$ states. Elastic impurity scattering implies $|\mathbf{q}| = |\mathbf{q}'|$. By Fermi's golden rule, $W_{\mathbf{q},\mathbf{q}'} = (2\pi/\hbar)|T_{\mathbf{q},\mathbf{q}'}|^2\delta(E_{qs} - E_{q's})$, with the T-matrix element $T_{\mathbf{q},\mathbf{q}'}$ for scattering from $\mathbf{q}$ to $\mathbf{q}'$. The transition rate can be expressed in terms of the disorder potential [Eq. (5)]. Combining Eqs. (28) and (29), the transport time of Dirac electrons in the Born approximation reads

$$\frac{1}{\tau(\mathbf{q})} = \int \frac{d^2\mathbf{q}'}{(2\pi)^2} W_{\mathbf{q},\mathbf{q}'}[1 - \cos(\mathbf{q}',\mathbf{q})], \tag{30}$$

where the in-scattering term contributes to the factor $\cos(\mathbf{q}',\mathbf{q}) = \mathbf{q}'\cdot\mathbf{q}/q^2 = \cos(\phi - \phi')$ that is associated with the ladder-vertex correction in the Kubo theory [43,52].

To lowest order in the scattering potential (thereby disregarding skew scattering as above) the transition probability in the upper band reads

$$\begin{aligned}|T_{\mathbf{q},\mathbf{q}'}|^2 &\approx \langle|\langle u_{q'+}|\hat{V}|u_{q+}\rangle|^2\rangle_{\rm imp}\\ &= nV_0^2|\langle u_{q'+}|u_{q+}\rangle|^2\\ &= nV_0^2\left(1 - \sin^2\theta\sin^2\frac{\phi-\phi'}{2}\right),\end{aligned} \tag{31}$$

leading to the electron transport relaxation time

$$\begin{aligned}\frac{1}{\tau} &= \int \frac{d^2\mathbf{q}'}{(2\pi)^2}\frac{2\pi}{\hbar}|T_{\mathbf{q},\mathbf{q}'}|^2[1-\cos(\phi-\phi')]\delta(E_F - E_{q'+})\\ &= \frac{1}{4\tau_{\rm e}}\left(1 + 3\xi^2M_z^2\right).\end{aligned} \tag{32}$$

This result reduces to the transport relaxation time of massless Dirac electrons $\tau = 4\tau_{\rm e}$ for $\xi M_z \to 0$. From Eq. (12), the transport time without the vertex correction is

$$\begin{aligned}\frac{1}{\tau^{\rm nv}} &= -2\,{\rm Im}\,\hat{\Sigma}^R\\ &= \int \frac{d^2\mathbf{q}'}{(2\pi)^2}\frac{2\pi}{\hbar}|T_{\mathbf{q},\mathbf{q}'}|^2\delta(E_F - E_{q'+})\\ &= \frac{1}{4\tau_{\rm e}}2\left(1 + \xi^2M_z^2\right),\end{aligned} \tag{33}$$

while the transport time with in-scattering is expressed as Eq. (32). On the other hand, Eq. (14) gives a corrected velocity (or current) of the form $v_x = sav\sin\theta\cos\phi$, with $a = \tau/\tau^{\rm nv}$,

which directly relates the ladder-vertex correction in the Kubo theory with the Boltzmann transport time [43]. Therefore, we can confirm that the ladder-vertex correction and in-scattering terms both renormalize the velocity in the same way.

B. Longitudinal and transverse conductivities

Here we calculate the charge current $\mathbf{J}_c$ driven by an in-plane electric field as a function of the exchange field direction $\mathbf{M}$ as shown in Fig. 1. The corresponding nonequilibrium distribution function is $f(\mathbf{q}) = f^{(0)}(\mathbf{q}) + g(\mathbf{q}) = f^{(0)}(\mathbf{q}) + e\tau(\partial f^{(0)}/\partial E_{qs})\mathbf{v}_{qs}\cdot\mathbf{E}$, where at zero temperature $f^{(0)}(\mathbf{q}) \approx \theta(E_F - E_{qs})$. To leading order in $\mathbf{E} = E_x\hat{\mathbf{x}}$

$$\sigma_{ix} = \frac{\mathbf{J}_c\cdot\hat{\mathbf{e}}_i}{E_x} = \frac{-e}{E_x}\sum_s\int\frac{d^2\mathbf{q}}{(2\pi)^2}g(\mathbf{q})\mathbf{v}_{qs}\cdot\hat{\mathbf{e}}_i, \tag{34}$$

where $\hat{\mathbf{e}}_i = \hat{\mathbf{x}}$ and $\hat{\mathbf{y}}$ and the electron velocity $\mathbf{v}_{qs} = \langle\psi_{qs}|\hat{\mathbf{v}}|\psi_{qs}\rangle$ is the expectation value of the velocity operator $\hat{\mathbf{v}} = (-i/\hbar)[\hat{\mathbf{r}},\hat{H}] = v_F\hat{\mathbf{z}}\times\hat{\boldsymbol{\sigma}}$ or the group velocity $\mathbf{v}_{qs} = v_x\hat{\mathbf{x}} + v_y\hat{\mathbf{y}}$, with $v_x = sv_F\sin\theta\cos\phi$ and $v_y = sv_F\sin\theta\sin\phi$. When the Fermi energy is above the gap, i.e., $E_F > \Delta$, the longitudinal and transverse conductivities are

$$\sigma_{xx} = 2\frac{e^2}{h}\frac{E_F\tau_e}{\hbar}\frac{1-\xi^2M_z^2}{1+3\xi^2M_z^2}, \tag{35}$$

$$\sigma_{xy} = 0. \tag{36}$$

In contrast to the linear response result, Eq. (25), σ_{xy} vanishes, because intrinsic (Berry phase) and side-jump scattering contributions are not included in Eq. (28). Sinitsyn *et al.* [43] demonstrated that and how the Boltzmann equation can be repaired to recover the diagrammatic results for the AHE. We can disregard this complication for the MR, the focus of the present study, since the intrinsic mechanism and the side-jump scattering (to leading order) do not contribute to longitudinal transport.

C. Current-induced spin polarization

Here we discuss the conductivities derived above in terms of current-induced torque to the magnetization [49] in the metallic regime ($E_F > \Delta$) [45,53]. The electric-field-driven nonequilibrium spin density or Edelstein effect [54,55] can be expressed by the Kubo formula as well as by the Boltzmann theory. For 2D massless Dirac electrons, the charge current is proportional to the spin operator, as can be seen from $\hat{\mathbf{j}} = -e\hat{\mathbf{v}} = -ev_F\hat{\mathbf{z}}\times\hat{\boldsymbol{\sigma}}$. Therefore, a nonzero steady-state charge current implies a finite spin density that can easily be found by multiplying the charge current by $-\hbar/(2ev_F)$, yielding

$$\langle\mathbf{s}\rangle = \sum_s\int\frac{d^2\mathbf{q}}{(2\pi)^2}g(\mathbf{q})\mathbf{s}(q,s), \tag{37}$$

where $\mathbf{s}(q,s) = (\hbar/2)\langle\psi_{qs}|\hat{\boldsymbol{\sigma}}_\perp|\psi_{qs}\rangle = -\hbar/(2ev_F)\hat{\mathbf{z}}\times\mathbf{v}(q,s)$, with $\hat{\boldsymbol{\sigma}}_\perp = (\hat{\sigma}_x,\hat{\sigma}_y)$, i.e., for $\mathbf{E} = E_x\hat{\mathbf{x}}$,

$$\langle s_x\rangle = 0,\ \langle s_y\rangle = -\frac{\hbar}{2}\frac{2eE_x}{hv_F}\frac{E_F\tau_e}{\hbar}\frac{1-\xi^2M_z^2}{1+3\xi^2M_z^2}. \tag{38}$$

The current-induced spin polarization is therefore not affected by an in-plane magnetization despite the exchange interaction in Eq. (1). Finite functional derivatives of the total energy as a function of $\mathbf{M}$ are equivalent to effective fields acting on the magnetization. From the exchange energy $E_{ex} = \Delta\langle\mathbf{s}\rangle\cdot\mathbf{M}$, we can compute the (fieldlike) $\mathbf{T} = -\gamma(\delta E_{ex}/\delta\mathbf{M})\times\mathbf{M} = -\gamma\Delta\langle s_y\rangle\hat{\mathbf{y}}\times\mathbf{M}$, where γ is the gyromagnetic ratio. When $\mathbf{M}\|\mathbf{E}$, the torque strives to rotate the magnetization *out-of-plane,* while it vanishes when $\mathbf{M}\|\hat{\mathbf{y}}$, just like the torques induced by the spin Hall effect in metallic conductors. However, the electric resistance is not affected because there is no *in-plane* (antidampinglike) torque. The M_z dependence of Eqs. (38) and (35) is the same, which is another consequence of the spin-momentum locking in the Dirac electron system.

V. MAGNETIC IMPURITIES

We assumed above nonmagnetic scattering which might not be a good representation of the TI | FI interface. Any roughness of this interface is likely to introduce magnetic disorder on the TI surface that can be modeled by randomly distributed magnetic impurities of spin S with the direction given by the unit vector $\mathbf{S}_{m,i}$ with index i at positions $\mathbf{R}_i$ and scattering potential

$$\hat{V}_m(\mathbf{r}) = V_m\sum_{i=1}^{N_m}\hat{\boldsymbol{\sigma}}\cdot\mathbf{S}_{m,i}\delta(\mathbf{r}-\mathbf{R}_i), \tag{39}$$

where $V_m = J_mS$ is the interaction strength between the conduction electrons and the local moments with a magnitude S and an exchange constant J_m. Since these impurities are coupled to the FI magnetization, a large fraction is likely to be parallel to $\mathbf{M}$. TI surface states with magnetic impurities (but without proximity ferromagnets) display various phases as a function of the impurity concentration and the temperature (here $T = 0$) [56,57]. For example, a phase transition from a paramagnetic to an out-of-plane ferromagnetic phase can be induced by increasing the impurity concentration. Only when the Ruderman-Kittel-Kasuya-Yosida (RKKY) interaction among impurity spins is overcome by the exchange interaction from the attached FI does the ferromagnetic phase become aligned to the FI magnetization.

Next we calculate the conductivity in the presence of magnetic impurities modeled by Eq. (39). Since we found in previous sections that the Kubo and Boltzmann theories give identical results for the conductivities, we use the latter (and simpler) method in the following.

A. Magnetic impurity aligned to M

First, the magnetic impurities are assumed to be aligned such that $\mathbf{S}_m^i = \mathbf{M}$. Hence, the scattering potential can be simplified to $\hat{V}_m(\mathbf{r}) = V_m\hat{\boldsymbol{\sigma}}\cdot\mathbf{M}\sum_i\delta(\mathbf{r}-\mathbf{R}_i)$. The impurity moments contribute an exchange potential, $\langle\hat{V}_m\rangle = \Delta_mM_z\hat{\sigma}_z$, to the the surface electrons, where $\Delta_m = n_mV_m$ [58], which can be added to the proximity exchange as $\tilde{\Delta} = \Delta + \Delta_m$.

The transition probabilities in the upper band are then

$$\left|T^{(\mathrm{m})}_{\mathbf{q},\mathbf{q}'}\right|^2 \approx \langle|\langle u_{q'+}|\hat{V}_{\mathrm{m}}|u_{q+}\rangle|^2\rangle_{\mathrm{imp}} = n_{\mathrm{m}}V_{\mathrm{m}}^2|\langle u_{q'+}|(\hat{\sigma}_x M_x + \hat{\sigma}_y M_y + \hat{\sigma}_z M_z)|u_{q+}\rangle|^2$$
$$= n_{\mathrm{m}}V_{\mathrm{m}}^2\sin^2\theta\left(M_x^2\sin^2\frac{\phi+\phi'}{2} + M_y^2\cos^2\frac{\phi+\phi'}{2} - M_xM_y\sin(\phi+\phi')\right)$$
$$+ n_{\mathrm{m}}V_{\mathrm{m}}^2M_z\cos\theta\sin\theta[M_x(\sin\phi+\sin\phi') - M_y(\cos\phi+\cos\phi')]$$
$$+ n_{\mathrm{m}}V_{\mathrm{m}}^2M_z^2\left(1-\sin^2\theta\cos^2\frac{\phi-\phi'}{2}\right). \tag{40}$$

The associated electron transport time becomes

$$\frac{1}{\tau_{\mathrm{m}}(\mathbf{q})} = \int\frac{d^2\mathbf{q}'}{(2\pi)^2}\frac{2\pi}{\hbar}\left|T^{(\mathrm{m})}_{\mathbf{q},\mathbf{q}'}\right|^2[1-\cos(\phi-\phi')]\delta(E_F - E_{q'+})$$
$$= \frac{1}{4\tau^{\mathrm{e}}_{\mathrm{m}}}\left(1-M_z^2\right)\left(1-\tilde{\xi}^2M_z^2\right)[2+\cos 2(\phi_M-\phi)]$$
$$+ \frac{1}{4\tau^{\mathrm{e}}_{\mathrm{m}}}2\tilde{\xi}M_z^2\sqrt{\left(1-M_z^2\right)\left(1-\tilde{\xi}^2M_z^2\right)}\sin(\phi_M-\phi)$$
$$+ \frac{1}{4\tau^{\mathrm{e}}_{\mathrm{m}}}M_z^2\left(3+\tilde{\xi}^2M_z^2\right), \tag{41}$$

where

$$\frac{\hbar}{\tau^{\mathrm{e}}_{\mathrm{m}}} = n_{\mathrm{m}}V_{\mathrm{m}}^2\int_0^\infty qdq\delta(E_F - E_{q+}) = 2\pi n_{\mathrm{m}}V_{\mathrm{m}}^2D(E_F) \tag{42}$$

defines the elastic scattering rate by magnetic impurities, $\tilde{\xi} = \tilde{\Delta}/E_F$, and $\phi_{\mathrm{M}}(=\alpha)$ is the polar angle of the magnetization. The $\mathbf{q}$ dependence is caused by spin-flip scattering due to the in-plane magnetic impurities that contribute to the transport relaxation through the spin-momentum locking.

To leading order in $\mathbf{E} = E_x\hat{\mathbf{x}}$,

$$\sigma^{(\mathrm{m})}_{ij} = e^2\sum_s\int\frac{d^2\mathbf{q}}{(2\pi)^2}\delta(E_F - E_{qs})\tau_{\mathrm{m}}(\mathbf{q})v_iv_j$$
$$= 2\frac{e^2}{h}\frac{E_F\tau^{\mathrm{e}}_{\mathrm{m}}}{\hbar}\int_0^{2\pi}\frac{d\phi}{2\pi}$$
$$\times\frac{F_{ij}(\phi)}{A - B\sin(\phi_{\mathrm{M}}-\phi) + \cos 2(\phi_{\mathrm{M}}-\phi)}, \tag{43}$$

where $F_{xx}(\phi) = 1+\cos 2\phi$, $F_{xy}(\phi) = \sin 2\phi$, $A = 2 + M_z^2(3+\tilde{\xi}^2M_z^2)/[(1-M_z^2)(1-\tilde{\xi}^2M_z^2)]$, and $B = 2\tilde{\xi}M_z^2/\sqrt{(1-M_z^2)(1-\tilde{\xi}^2M_z^2)}$. In the absence of out-of-plane spin components $M_z = 0$ $(A = 2, B = 0)$,

$$\sigma^{(\mathrm{m})}_{xx} = 2\frac{e^2}{h}\frac{E_F\tau^{\mathrm{e}}_{\mathrm{m}}}{\hbar}\frac{\sqrt{3}}{3}\left[1-(2-\sqrt{3})\left(M_x^2-M_y^2\right)\right], \tag{44}$$

$$\sigma^{(\mathrm{m})}_{xy} = 2\frac{e^2}{h}\frac{E_F\tau^{\mathrm{e}}_{\mathrm{m}}}{\hbar}\frac{2\sqrt{3}}{3}(2-\sqrt{3})M_xM_y. \tag{45}$$

In contrast to the homogeneous proximity effect, a disordered in-plane exchange potential generates a MR with periodicity π as well as a planar Hall effect. This result agrees with the AMR computed for a single magnetic impurity by first principles [59] and explains the experimental in-plane MR of TI/FI bilayers [60] as well as magnetically doped TIs [61]. The reported in-plane unidirectional MR (with periodicity 2π) in the TI/magnetically doped TI bilayer [62] is nonlinear (proportional to the applied current), and therefore beyond the linear response treatment here. In Fig. 5(b), the planar Hall conductivity is plotted as a function of the in-plane magnetization angle α that displays both AMR and SMR character. The planar Hall angle

$$\theta_{\mathrm{PHE}} \equiv \frac{\sigma^{(\mathrm{m})}_{xy}}{\sigma^{(\mathrm{m})}_{xx}} = \frac{\sin 2\alpha}{(2+\sqrt{3}) - \cos 2\alpha} \leqslant 0.28 \tag{46}$$

is maximal for $\alpha = \tan^{-1}(3^{-1/4}) = 37.2^\circ$. This Hall angle for diffuse transport is much smaller than that predicted in a ballistic transport model [63].

In Fig. 5 we plot the conductivity equation, Eq. (43), as a function of the angles α, β, and γ as defined in Fig. 4, where $\alpha = \phi_{\mathrm{M}}$ is the in-plane angle, while β and γ are out-of-plane angles θ_{M} for $\alpha = \pi/2$ and $\alpha = 0$, respectively. A sizable MR with twofold symmetry in all three orthogonal planes is shown in Fig. 4(d). In Fig. 5(a), the conductivity σ_{xx} [see Eq. (45)] depends only on the in-plane magnetization angle ϕ_{M}, which can be explained in terms of electron scattering by the magnetic impurities under spin-momentum

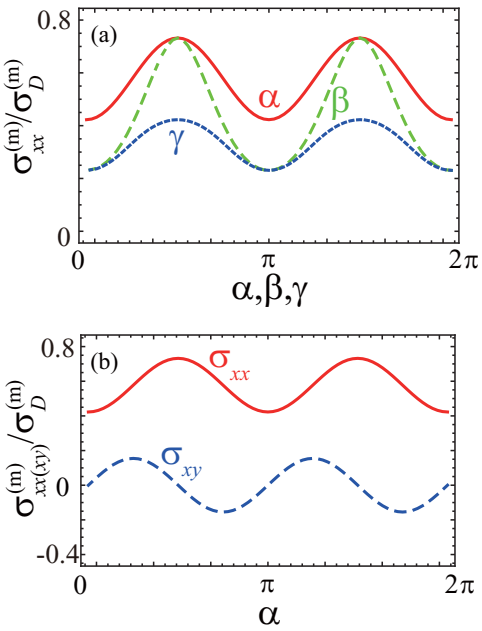

FIG. 5. (a) MR curves for a TI|FI bilayer as a function of magnetization angles α, β, and γ [defined in Fig. 4(d)] for $\tilde{\xi} = 0.5$. $\sigma^{(\mathrm{m})}_D = (2e^2/h)(E_F\tau^{\mathrm{e}}_{\mathrm{m}}/\hbar)$ is the longitudinal conductivity limited by magnetic impurities. (b) Longitudinal and transverse conductivities as a function of in-plane magnetization angles α.

locking of the Dirac electrons. When the magnetic impurities are aligned with $\mathbf{M}$, electron scattering is affected by the magnetization of the FI and the transport time is modified. In contrast to the MR by nonmagnetic impurities, the out-of-plane conductivities $\sigma_{xx}(\beta)$ and $\sigma_{xx}(\gamma)$ differ, which again reflects the spin-momentum locking of Dirac electrons, i.e., fixing the spin direction to $0\,(\pi/2)$ leads to different momentum relaxations.

When the magnetic impurity concentration becomes higher, the impurity spin direction may be locked perpendicular to the plane by the RKKY coupling mediated by the Dirac electrons, which is stabilized by the induced gap [56,57]. Weak applied magnetic fields then control only the direction of FI magnetization; only a sufficiently strong magnetic field may also rotate the orientation of the impurity magnetization from the z direction. In the former regime $\hat{V}_{\rm m}(\mathbf{r}) = V_{\rm m}\hat{\sigma}_z \sum_i \delta(\mathbf{r} - \mathbf{R}_i)$ and $\langle \hat{V}_{\rm m}\rangle = \Delta_{\rm m}\hat{\sigma}_z$ with upper-band transition probabilities

$$\left|T^{(\rm z)}_{\mathbf{q},\mathbf{q}'}\right|^2 = n_{\rm m}V_{\rm m}^2\left(1 - \sin^2\theta\cos^2\frac{\phi-\phi'}{2}\right), \tag{47}$$

which lead to the following transport time and longitudinal conductivity:

$$\frac{1}{\tau_z} = \frac{1}{4\tau^e_{\rm m}}\left(3 + \xi_{\rm m}^2 + \xi^2 M_z^2\right), \tag{48}$$

$$\sigma^{(\rm z)}_{xx} = 2\frac{e^2}{h}\frac{E_F\tau^{\rm e}_{\rm m}}{\hbar}\frac{1 - \xi_{\rm m}^2 - \xi^2M_z^2}{3 + \xi_{\rm m}^2 + \xi^2M_z^2}, \tag{49}$$

with $\xi_{\rm m} = \Delta_{\rm m}/E_F$. The conductivity is now reduced because by scattering at a magnetic impurity the electron acquires a phase shift, $e^{i(\phi+\pi)}$, that enhances backscattering.

B. Paramagnetic impurities

When the magnetic impurities are paramagnetic, $\mathbf{S}^i_{\rm m} = \mathbf{S}_{\rm m}$, and assuming that the magnetic fields do not significantly polarize the moments $\langle \mathbf{S}_{\rm m}\rangle = 0$, the scattering potential is reduced to $\hat{V}_{\rm m}(\mathbf{r}) = V_{\rm m}\sum_i \hat{\boldsymbol{\sigma}}\cdot\mathbf{S}_{{\rm m},i}\delta(\mathbf{r} - \mathbf{R}_i)$. The transition amplitude in the upper band becomes

$$\begin{aligned}\left|T^{(\rm p)}_{\mathbf{q},\mathbf{q}'}\right|^2 &\approx \langle|\langle u_{q'+}|\hat{V}_{\rm m}|u_{q+}\rangle|^2\rangle_{\rm imp}\\ &= n_{\rm m}V_{\rm m}^2|\langle u_{q'+}|\hat{\boldsymbol{\sigma}}\cdot\mathbf{S}_{\rm m}|u_{q+}\rangle|^2\\ &= n_{\rm m}V_{\rm m}^2\frac{1}{3}S^2\left(1 + \sin^2\theta\sin^2\frac{\phi-\phi'}{2}\right).\end{aligned} \tag{50}$$

The electron transport time is

$$\frac{1}{\tau_{\rm p}} = \frac{1}{12\tau^{\rm e}_{\rm m}}S^2\left(5 - 3\xi^2M_z^2\right). \tag{51}$$

An in-plane component $(S_{{\rm m},i})_{x(y)}$ contributes to the transport relaxation. To leading order in $\mathbf{E} = E_x\hat{\mathbf{x}}$,

$$\sigma^{(\rm p)}_{xx} = 2\frac{e^2}{h}\frac{E_F\tau^{\rm e}_{\rm m}}{\hbar S^2}\frac{3\left(1 - \xi^2M_z^2\right)}{5 - 3\xi^2M_z^2}. \tag{52}$$

The z component of the magnetic impurity contributes a scattering phase shift $e^{i(\phi+\pi)}$ and thereby additional backscattering. Moreover, the x and y components of the magnetic impurity locally break the time-reversal symmetry on the TI surface and allow backscattering, which is weaker than for the polarized impurities, however.

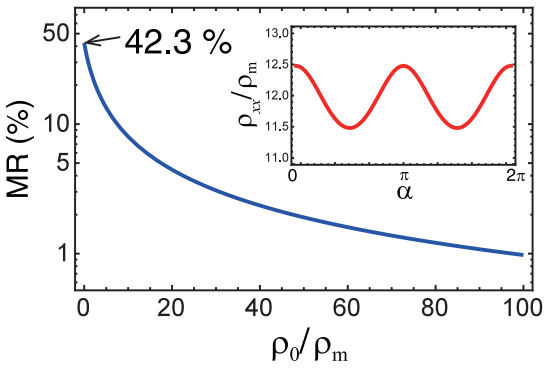

FIG. 6. In-plane MR ratio as a function of normalized nonmagnetic resistivity $\rho_0/\rho_{\rm m}$, where $\rho_0 = \sigma_D^{-1}$ and $\rho_{\rm m} = (\sigma_D^{(\rm m)})^{-1}$. The inset shows the resistivity ρ_{xx} as a function of α for $\rho_0/\rho_{\rm m} = 10$.

C. In-plane magnetoresistance

The magnitude of the in-plane magnetoresistance can be expressed in terms of the MR ratio:

$$\mathrm{MR} = \frac{\rho_{xx}(\alpha = 0) - \rho_{xx}(\alpha = \pi/2)}{\rho_{xx}(\alpha = 0)}, \tag{53}$$

where $\rho_{xx} = \sigma_{xx}/(\sigma_{xx}^2 + \sigma_{xy}^2)$ is the resistivity. For comparison with experiments, we assume disorder with both nonmagnetic and magnetic impurities, Eqs. (5) and (39). Figure 6 is a plot of the in-plane MR ratio as a function of the normalized nonmagnetic resistivity $\rho_0/\rho_{\rm m}$, where $\rho_0 = \sigma_D^{-1}$ and $\rho_{\rm m} = (\sigma_D^{(\rm m)})^{-1}$. The MR ratio can become 42.3% in the absence of nonmagnetic scattering $\rho_0 = 0$, but gradually decreases with increasing $\rho_0/\rho_{\rm m}$. Reference [60] reports a measured MR $\sim 3\%$ for a TI|YIG system, while Ref. [62] finds MR $\sim$ 13% for TI|magnetically doped TI bilayers. In the inset of Fig. 6, we plot the resistivity ρ_{xx} as a function of α for $\rho_0/\rho_{\rm m} = 10$, in good agreement with the measured in-plane MR of TI|CoFeB bilayers [64].

VI. SUMMARY

We model the magnetic-proximity-induced magnetoresistance in disordered topological|ferromagnetic insulator bilayers. Assuming that an FI contact magnetizes the TI-surface states, we derive analytical expressions for the electric dc conductivity. We formulate electron transport by the Kubo linear response theory including the ladder-vertex correction as well as by the Boltzmann approach including the in-scattering term of the collision integral. The induced exchange splitting generates an electric resistance that depends on the normal component of the magnetization direction for nonmagnetic disorder. For in-plane magnetizations, unlike for the magnetic Rashba 2D system, the in-plane MR then vanishes. For out-of-plane magnetizations, we predict that the gap opening at the Dirac point causes a large MR ratio. On the other hand, we do find an in-plane MR and planar Hall effect in the presence of magnetic impurities aligned to the FI magnetization that can be explained by the spin-momentum locking for Dirac electrons. Our calculated results agree with the limited number of experiments on the out-of-plane MR. We explain the MR

observed for in-plane magnetizations by magnetic disorder, which thereby provides information on the interface morphology. In terms of the functional dependence on magnetization direction, our model predicts a mixture of AMR and SMR character. Our model calculation might help the theoretical design of topological insulators for next-generation spin-based information technologies.

ACKNOWLEDGMENTS

The authors thank Y. Araki, K. Nomura, Y. Ominato, I. Matsuzaki, D. Kurebayashi, Y. Shiomi, J. Inoue, and M. Titov for valuable discussions. This work was supported by Grants-in-Aid for Scientific Research (Grants No. 25247056, No. 25220910, and No. 268063) from the JSPS, the FOM (Stichting voor Fundamenteel Onderzoek der Materie), the ICC-IMR, EU-FET Grant InSpin No. 612759, and the DFG Priority Programme 1538 "Spin-Caloric Transport" (Grant No. BA 2954/2).

APPENDIX: CURRENT-INDUCED SPIN POLARIZATION IN THE PRESENCE OF MAGNETIC DISORDER

Here we calculate the electric-field-driven nonequilibrium spin density in the presence of magnetic impurities [Eq. (39)] by the Boltzmann theory. A nonzero steady-state charge current implies a finite spin density that can easily be found by multiplying the charge current by $-\hbar/(2ev_F)$, yielding

$$\langle \mathbf{s} \rangle = e \sum_s \int \frac{d^2\mathbf{q}}{(2\pi)^2} \delta(E_F - E_{qs}) \tau_{\mathrm{m}}(\mathbf{q}) (\mathbf{v}_{qs} \cdot \mathbf{E}) \mathbf{s}_{qs}, \quad \text{(A1)}$$

where $\mathbf{s}_{qs} = -\hbar/(2ev_F)\hat{\mathbf{z}} \times \mathbf{v}_{qs}$. In the presence of an electric field $\mathbf{E} = E_x\hat{\mathbf{x}}$ and for in-plane magnetizations,

$$\langle \mathbf{s} \rangle = -\frac{\hbar}{2} \frac{2eE_x}{hv_F} \frac{E_F \tau_{\mathrm{m}}^{\mathrm{e}}}{\hbar} \frac{\sqrt{3}}{3} \big[-2(2-\sqrt{3}) M_x M_y \hat{\mathbf{x}} + \big[1 - (2-\sqrt{3}) \big(M_x^2 - M_y^2 \big) \big] \hat{\mathbf{y}} \big]. \quad \text{(A2)}$$

In contrast to the current-induced spin polarization for the normal disorder, Eq. (A2) is affected by an in-plane magnetization through the exchange interaction in Eq. (39).

[1] I. Žutić, J. Fabian, and S. Das Sarma, Rev. Mod. Phys. **76**, 323 (2004); A. Hoffmann and S. D. Bader, Phys. Rev. Appl. **4**, 047001 (2015).
[2] T. McGuire and R. Potter, IEEE Trans. Magn. **11**, 1018 (1975).
[3] J. Schliemann and D. Loss, Phys. Rev. B **68**, 165311 (2003).
[4] K. Výborný, A. A. Kovalev, J. Sinova, and T. Jungwirth, Phys. Rev. B **79**, 045427 (2009).
[5] T. Kato, Y. Ishikawa, H. Itoh, and J.-I. Inoue, Phys. Rev. B **77**, 233404 (2008).
[6] A. A. Kovalev, Y. Tserkovnyak, K. Výborný, and J. Sinova, Phys. Rev. B **79**, 195129 (2009).
[7] H. Nakayama, M. Althammer, Y.-T. Chen, K. Uchida, Y. Kajiwara, D. Kikuchi, T. Ohtani, S. Geprags, M. Opel, S. Takahashi, R. Gross, G. E. W. Bauer, S. T. B. Goennenwein, and E. Saitoh, Phys. Rev. Lett. **110**, 206601 (2013).
[8] Y.-T. Chen, S. Takahashi, H. Nakayama, M. Althammer, S. T. B. Goennenwein, E. Saitoh, and G. E. W. Bauer, Phys. Rev. B **87**, 144411 (2013).
[9] J. Sinova, S. O. Valenzuela, J. Wunderlich, C. H. Back, and T. Jungwirth, Rev. Mod. Phys. **87**, 1213 (2015).
[10] B. F. Miao, S. Y. Huang, D. Qu, and C. L. Chien, Phys. Rev. Lett. **112**, 236601 (2014).
[11] V. L. Grigoryan, W. Guo, G. E. W. Bauer, and J. Xiao, Phys. Rev. B **90**, 161412(R) (2014).
[12] S. S.-L. Zhang, G. Vignale, and S. Zhang, Phys. Rev. B **92**, 024412 (2015).
[13] C. O. Avci, K. Garello, A. Ghosh, M. Gabureac, S. F. Alvarado, and P. Gambardella, Nat. Phys. **11**, 570 (2015).
[14] J. Kim, P. Sheng, S. Takahashi, S. Mitani, and M. Hayashi, Phys. Rev. Lett. **116**, 097201 (2016).
[15] M. Z. Hasan and C. L. Kane, Rev. Mod. Phys. **82**, 3045 (2010).
[16] X.-L. Qi and S.-C. Zhang, Rev. Mod. Phys. **83**, 1057 (2011).
[17] Y. Ando, J. Phys. Soc. Jpn. **82**, 102001 (2013).
[18] C. H. Li, O. M. J. van 't Erve, J. T. Robinson, Y. Liu, L. Li, and B. T. Jonker, Nat. Nanotechnol. **9**, 218 (2014).
[19] Y. Shiomi, K. Nomura, Y. Kajiwara, K. Eto, M. Novak, K. Segawa, Y. Ando, and E. Saitoh, Phys. Rev. Lett. **113**, 196601 (2014).
[20] K. Kondou, R. Yoshimi, A. Tsukazaki, Y. Fukuma, J. Matsuno, K. S. Takahashi, M. Kawasaki, Y. Tokura, and Y. Otani, Nat. Phys. **12**, 1027 (2016).
[21] A. A. Burkov, A. S. Núñez, and A. H. MacDonald, Phys. Rev. B **70**, 155308 (2004).
[22] T. Yokoyama, Y. Tanaka, and N. Nagaosa, Phys. Rev. B **81**, 121401(R) (2010).
[23] A. A. Burkov and D. G. Hawthorn, Phys. Rev. Lett. **105**, 066802 (2010).
[24] Z. Jiang, F. Katmis, C. Tang, P. Wei, J. S. Moodera, and J. Shi, Appl. Phys. Lett. **104**, 222409 (2014).
[25] Y. Ando, T. Hamasaki, T. Kurokawa, K. Ichiba, F. Yang, M. Novak, S. Sasaki, K. Segawa, Y. Ando, and M. Shiraishi, Nano. Lett. **14**, 6226 (2014).
[26] Y. Fan, P. Upadhyaya, X. Kou, M. Lang, S. Takei, Z. Wang, J. Tang, L. He, L.-T. Chang, M. Montazeri, G. Yu, W. Jiang, T. Nie, R. N. Schwartz, Y. Tserkovnyak, and K. L. Wang, Nat. Mater. **13**, 699 (2014).
[27] A. R. Mellnik, J. S. Lee, A. Richardella, J. L. Grab, P. J. Mintun, M. H. Fischer, A. Vaezi, A. Manchon, E.-A. Kim, N. Samarth, and D. C. Ralph, Nature (London) **511**, 449 (2014).
[28] Z. Jiang, C.-Z. Chang, M. R. Masir, C. Tang, Y. Xu, J. S. Moodera, A. H. MacDonald, and J. Shi, Nat. Commun. **7**, 11458 (2016)
[29] H. Wang, J. Kally, J. S. Lee, T. Liu, H. Chang, D. R. Hickey, K. A. Mkhoyan, M. Wu, A. Richardella, and N. Samarth, Phys. Rev. Lett. **117**, 076601 (2016).
[30] Z. Jiang, C. Chang, C. Tang, P. Wei, J. S. Moodera, and J. Shi, Nano Lett. **40**, 5835 (2015).
[31] Z. Wang, C. Tang, R. Sachs, Y. Barlas, and J. Shi, Phys. Rev. Lett. **114**, 016603 (2015).

[32] J. C. Leutenantsmeyer, A. A. Kaverzin, M. Wojtaszek, and B. J. van Wees, 2D Mater. **4**, 014001 (2016).
[33] P. Wei, S. Lee, F. Lemaitre, L. Pinel, D. Cutaia, W. Cha, F. Katmis, Y. Zhu, D. Heiman, J. Hone, J. S. Moodera, and C.-T. Chen, Nat. Mater. **15**, 711 (2016).
[34] Y. Tserkovnyak, A. Brataas, G. E. W. Bauer, and B. I. Halperin, Rev. Mod. Phys. **77**, 1375 (2005).
[35] X. Jia, K. Liu, K. Xia, and G. E. W. Bauer, Europhys. Lett. **96**, 17005 (2011).
[36] A. Hallal, F. Ibrahim, H. X. Yang, S. Roche, and M. Chshiev, 2D Mater. (2017), doi:10.1088/2053-1583/aa6663.
[37] K. Nomura and N. Nagaosa, Phys. Rev. B **82**, 161401(R) (2010).
[38] V. K. Dugaev, P. Bruno, M. Taillefumier, B. Canals, and C. Lacroix, Phys. Rev. B **71**, 224423 (2005).
[39] J. I. Inoue, T. Kato, Y. Ishikawa, H. Itoh, G. E. W. Bauer, and L. W. Molenkamp, Phys. Rev. Lett. **97**, 046604 (2006).
[40] T. S. Nunner, N. A. Sinitsyn, M. F. Borunda, V. K. Dugaev, A. A. Kovalev, A. Abanov, C. Timm, T. Jungwirth, J.-I. Inoue, A. H. MacDonald, and J. Sinova, Phys. Rev. B **76**, 235312 (2007).
[41] J. Inoue, G. E. W. Bauer, and L. W. Molenkamp, Phys. Rev. B **70**, 041303(R) (2004).
[42] N. A. Sinitsyn, J. E. Hill, H. Min, J. Sinova, and A. H. MacDonald, Phys. Rev. Lett. **97**, 106804 (2006).
[43] N. A. Sinitsyn, A. H. MacDonald, T. Jungwirth, V. K. Dugaev, and J. Sinova, Phys. Rev. B **75**, 045315 (2007).
[44] I. A. Ado, I. A. Dmitriev, P. M. Ostrovsky, and M. Titov, Europhys. Lett. **111**, 37004 (2015).
[45] P. B. Ndiaye, C. A. Akosa, M. H. Fischer, A. Vaezi, E.-A. Kim, and A. Manchon, arXiv:1509.06929.
[46] N. H. Shon and T. Ando, J. Phys. Soc. Jpn. **67**, 2421 (1998).
[47] D. Culcer, E. H. Hwang, T. D. Stanescu, and S. Das Sarma, Phys. Rev. B **82**, 155457 (2010).
[48] D. Culcer and S. Das Sarma, Phys. Rev. B **83**, 245441 (2011).
[49] A. Sakai and H. Kohno, Phys. Rev. B **89**, 165307 (2014).
[50] A. Sabzalipour, J. Abouie, and S. H. Abedinpour, J. Phys.: Condens. Matter **27**, 115301 (2015).
[51] S. Adam, P. W. Brouwer, and S. Das Sarma, Phys. Rev. B **79**, 201404(R) (2009).
[52] G. Rickayzen, *Green's Functions and Condensed Matter* (Academic, London, 1984).
[53] I. Garate and M. Franz, Phys. Rev. Lett. **104**, 146802 (2010).
[54] V. M. Edelstein, Solid State Commun. **73**, 233 (1990).
[55] J. Inoue, G. E. W. Bauer, and L. W. Molenkamp, Phys. Rev. B **67**, 033104 (2003).
[56] Q. Liu, C.-X. Liu, C. Xu, X.-L. Qi, and S.-C. Zhang, Phys. Rev. Lett. **102**, 156603 (2009).
[57] H. Ochoa, Phys. Rev. B **92**, 081410(R) (2015).
[58] K. Nomura and N. Nagaosa, Phys. Rev. Lett. **106**, 166802 (2011).
[59] A. Narayan, I. Rungger, and S. Sanvito, New J. Phys. **17**, 033021 (2015).
[60] K. Banerjee, J. Besbas, P. Ren, L. Wang, and H. Yang, Phys. Status Solidi RRL **9**, 175 (2015).
[61] A. Kandala, A. Richardella, S. Kempinger, C.-X. Liu, and N. Samarth, Nat. Commun. **6**, 7434 (2015).
[62] K. Yasuda, A. Tsukazaki, R. Yoshimi, K. S. Takahashi, M. Kawasaki, and Y. Tokura, Phys. Rev. Lett. **117**, 127202 (2016).
[63] B. Scharf, A. Matos-Abiague, J. E. Han, E. M. Hankiewicz, and I. Žutić, Phys. Rev. Lett. **117**, 166806 (2016).
[64] Y. Lv, J. Kally, D. Zhang, J. S. Lee, M. Jamali, N. Samarth, and J.-P. Wang, arXiv:1701.06505.